energies

Article

Performance Assessment of Double Corrugated Tubes in a Tube-In-Shell Heat Exchanger

Kristina Navickaitė [1,*], Michael Penzel [1], Christian R. H. Bahl [2] and Kurt Engelbrecht [2]

[1] Beckmann-Institut für Technologieentwicklung e.V., Annaberger Str. 73, 09111 Chemnitz, Germany; michael.penzel@beckmann-institut.de
[2] Department of Energy Conversion and Storage, Technical University of Denmark, Anker Engelunds Vej, 2800 Kongens Lyngby, Denmark; chrb@dtu.dk (C.R.H.B.); kuen@dtu.dk (K.E.)
* Correspondence: navickaite@beckmann-institut.de

Abstract: In this article, the performance of double corrugated tubes applied in a tube-in-shell heat exchanger is analysed and compared to the performance of a heat exchanger equipped with straight tubes. The CFD (computational fluid dynamics) analysis was performed considering a turbulent flow regime at several mass flow rates. It is observed that the double corrugated geometry does not have a significant impact on the pressure drop inside the analysed heat exchanger, while it has the potential to increase its thermal performance by up to 25%. The *ε–NTU* (effectiveness–number of transfer units) relation also demonstrates the advantage of using double corrugated tubes in tube-in-shell heat exchangers over straight tubes.

Keywords: nature inspired geometry; enhanced heat transfer; turbulent flow region; CFD modelling

check for updates

Citation: Navickaitė, K.; Penzel, M.; Bahl, C.R.H.; Engelbrecht, K. Performance Assessment of Double Corrugated Tubes in a Tube-In-Shell Heat Exchanger. *Energies* **2021**, *14*, 1343. https://doi.org/10.3390/en14051343

Academic Editor: Luiz C. Wrobel

Received: 27 January 2021
Accepted: 22 February 2021
Published: 1 March 2021

1. Introduction

Heat exchangers (HEXs) are used in a wide range of engineering applications, from the food industry [1] to civil engineering and aviation [2]. Improving HEX performance is the subject of continuous research addressing energy efficiency issues [3]. The research efforts to enhance the heat transfer performance can be divided into three main categories. Namely, the active approach that requires an external power input, such as electric energy [4,5], the passive approach that deals with modified surfaces [6–8] and a combined approach where advantages of the active and passive methods are combined.

Passive methods have attracted the largest attention among researchers, due to the fact that there is no additional power input required to achieve the heat transfer enhancement. Multiple studies on different augmented and/or coated surfaces [6], e.g., tubes with fitted inserts [9–12], grooved surfaces [13–15] and structured microchannels [16] have been reported. Various types of corrugations have been analysed as well; for instance, tubes with multiple starts [17], tubes with alternating ellipse axes [18,19] and double corrugated tubes with constant hydraulic diameter, D_h, or constant cross-section area, A_c, [20,21]. All of the reported numerical and/or experimental studies have demonstrated a significant increase in heat transfer inside the tube geometry with higher or lower increase in pressure drop compared to a baseline case. However, none of these studies report results of heat transfer and pressure drop on the outside of the tube for a tube-in-shell HEX application.

One of the reasons for the lack of available scientific data on tube-in-shell heat exchanger performance is that a comprehensive experimental analysis is expensive and time-consuming [22]. Numerical modelling of such systems is also resource intensive [3], as a model of a realistic tube-in-shell HEX including baffles, tube-baffle and baffle-shell leakage, flow bypass etc., would require a sufficiently fine mesh to capture the design details, and thus tremendous computing power [3,22]. Therefore, some approximations and assumptions have been made in order to simplify the HEX modelling while still obtaining a meaningful comparison. For example, a distributed resistance model was developed to imply the flow resistance on the shell side that is equivalent to the resistance caused by a tube bundle [22]. The tube-baffle and baffle-shell leakage were accounted for by employing the Bernoulli equation with losses along the streamline [22]. The results obtained in [22,23] were compared to the experimental results used to develop the Bell–Delaware method for heat exchanger rating and were within 15% agreement. However, one of the limitations of this approach is that the model would not take into consideration an impact of the tube geometry on the performance of a HEX.

Another modelling approach is to model a representative segment of a tube-in-tube heat exchanger [24]. A segment of a coiled tube-in-tube heat exchanger with water–water counter-flow was studied in [24]. The simulation results were compared to the experimental results on a coiled tube-in-tube heat exchanger and were within 4% and 10% agreement for the inner and the outer tubes, respectively [24].

The third way to model the performance of a heat exchanger is presented in [25]. There, the tube side is assumed to be solid rods with constant wall temperature, while the shell side is modelled using a non-isothermal turbulent flow model. The shell side was equipped with six baffles, and the tubes were arranged in a triangular pitch. The influence of the baffle spacing and baffle cut on the performance of a counter flow HEX is discussed in the study [25]. Moreover, the suitability of various turbulence models for modelling a tube-in-shell HEX was addressed as well. The obtained simulation results were compared to the Kern and Bell–Delaware methods. It was concluded that the Kern method always under-predicts the performance of a HEX, while the Bell–Delaware method agrees very well with the developed CFD model [25]. It was also concluded that the first order k-ε realisable turbulence model is the most suitable modelling approach for the study in [25].

In the present study, the modelling approach presented in [25] was chosen to model the performance of double corrugated tubes in a tube-in-shell heat exchanger. The CFD results obtained in the present study are validated against the CFD results presented in [25], which was validated against the Bell–Delaware and Kern methods. The Bell–Delaware method was developed for rating real heat exchangers and accounting for tube-baffle and baffle-shell leakage as well as uneven baffle spacing and unevenness of the tube wall dimensions [26]. The purpose of this study is to characterise the relative performance of double corrugated tubes in HEXs. Therefore, a small HEX was modelled with straight and with double corrugated tubes in order to compare the performance of the enhanced geometry to the reference straight geometry. To do so, the number of transfer units, *NTU*, method was employed, since it is a simple and convenient way to characterise HEXs [26].

2. Materials and Methods

The experimental and CFD simulation results on double corrugated tube geometry were first presented in [20,21], respectively. There, the enhancement of the heat transfer was numerically and experimentally analysed for internal flow. The double corrugation of the tube wall was shown to break up the thermal boundary layers and hinder their development, thus increasing the heat transfer through the tube wall at a reasonable increase in pressure drop [20,21]. The geometry of these double corrugated tubes mimics the blood vessels in counter flow heat exchangers existing in warm-blooded fish [27] and those fish species that are able to maintain their regional body temperature higher than that of their living environment [28]. The double corrugated tubes were divided into two main groups. Namely, double corrugated tubes with constant hydraulic diameter (EDH) and double corrugated tubes with constant cross-section area (EAC). The geometry of the double corrugated tubes is defined by Equations (1) and (2) for EDH and EAC tubes, respectively [21].

$$\begin{cases} x = \frac{R}{2} AR^{\sin\left(\frac{2\pi}{k} z\right)} + \frac{R}{2} \\ y = \frac{R}{2} AR^{-\sin\left(\frac{2\pi}{k} z\right)} + \frac{R}{2} \end{cases} \tag{1}$$

$$\begin{cases} x = R \cdot AR^{\frac{\sin\left(\frac{2\pi}{k} z\right)}{2}} \\ y = R \cdot AR^{\frac{-\sin\left(\frac{2\pi}{k} z\right)}{2}} \end{cases} \tag{2}$$

where R is the radius of an equivalent straight tube, AR is the aspect ratio between the x and y axis, z is the coordinate in the direction of the tube length and k is the corrugation period.

From Equations (1) and (2), one can see that the cross-section of double corrugated tubes is periodically a circle.

In this study, eight double corrugated tubes that demonstrated the best experimental results reported in [20,29] have been selected for modelling their overall performance in a tube-in-shell heat exchanger considering the shell side. Namely, four EDH and four EAC type of tubes with AR = 1.6 and AR = 2.0 and with $k = 1.5 \cdot D_h$ and $k = 3.0 \cdot D_h$, where D_h = 20 mm have been selected to correspond to [25]. A differential volume of each double corrugated tube, selected for this study, is shown in Figure 1.

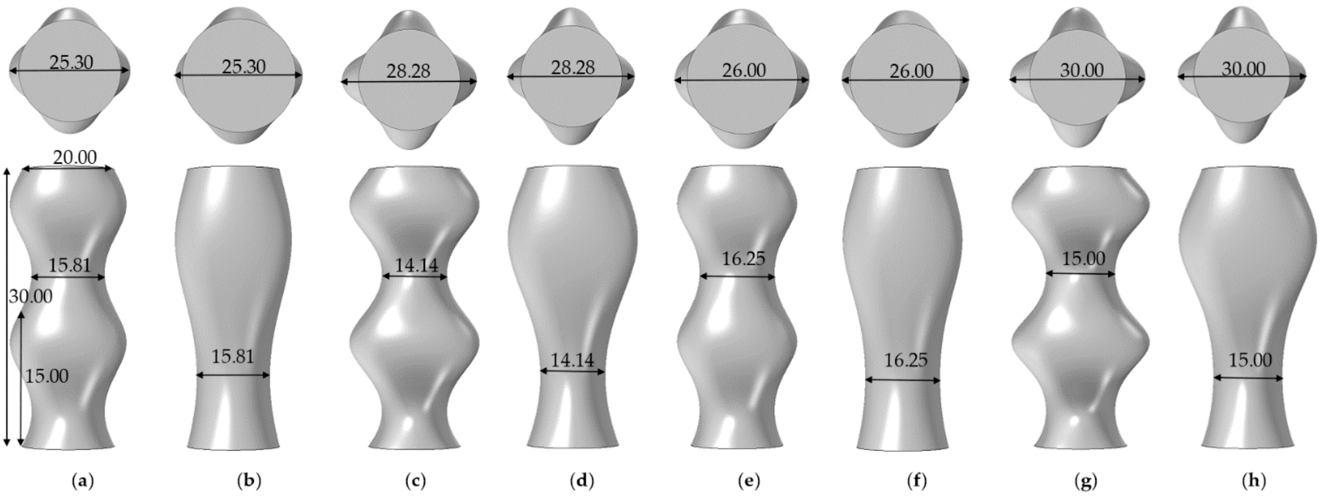

Figure 1. A segment of a double corrugated tube: (**a**) EAC AR16 K15D, (**b**) EAC AR16 K30D, (**c**) EAC AR20 K15D, (**d**) EAC AR20 K30D, (**e**) EDH AR16 K15D, (**f**) EDH AR16 K30D, (**g**) EDH AR20 K15D and (**h**) EDH AR20 K30D. All dimensions are given in millimetres. EAC: double corrugated tubes with constant cross-section area, EDH: double corrugated tubes with constant hydraulic diameter, AR: aspect ratio between the x and y axis.

Comparing two double corrugated tubes with the same aspect ratio AR, but one being EAC type and the other EDH, one can see that the geometry of EDH tubes is more tweaked. For example, the max/min values of the x/y axis are larger for EDH type of tubes compared to EAC ones, providing much sharper transition between peaks and valleys of the geometry. Therefore EDH-type tubes affect the fluid flow more, resulting in higher thermal performance and larger increase in pressure drop at the same operational conditions compared to the straight tube and also to the EAC type of tubes [20,29]. Nevertheless, the performance evaluation criterion, *PEC*, is higher for the EDH-type tubes compared to the EAC-type tubes [29].

In order to validate the CFD model used in this study, a model used in [25] was reconstructed and simulated using the same boundary conditions, mesh density and the turbulence model that was concluded to provide the best results. Namely, a tube-in-shell heat exchanger geometry with seven straight tubes arranged in triangular pitch with 30 mm distance was constructed using COMSOL Multiphysics (Version 5.5, COMSOL Multiphysics, Stockholm, Sweden). Figure 2 shows the geometrical arrangement of the reconstructed heat exchanger.

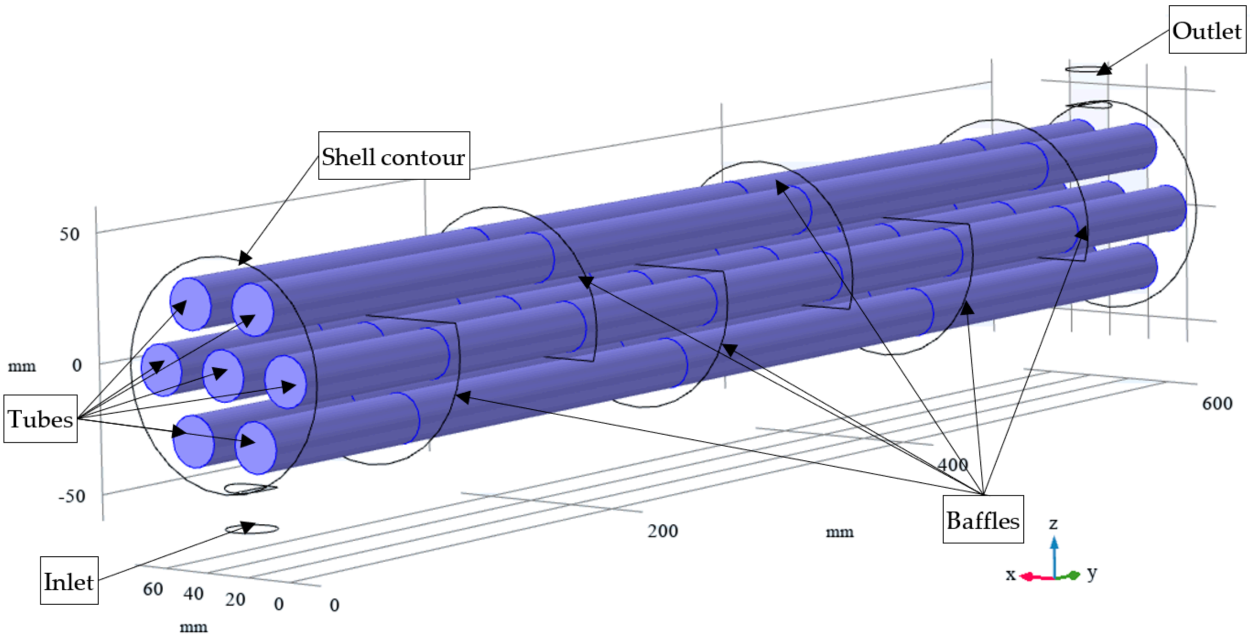

Figure 2. A tube-in-shell heat exchanger geometry reconstructed from [25].

The suitability of a symmetry boundary condition (BC) to minimise the computational efforts has been investigated as well. For this purpose, the reconstructed HEX model was split in half with a symmetry BC applied on the cut plane and then modelled again.

Once the developed model was validated against the reconstructed model, the geometrical arrangement of the analysed HEX was slightly modified to accommodate the double corrugated tubes as shown in Figure 3. A reference heat exchanger consisting of straight tubes was also modelled using the modified arrangement. As one can see from Figure 3, the tubes have a staggered arrangement, referred to as a 45° rotated square [26]. The difference in the tube arrangement in the present study and the one reported in [25] is schematically depicted in Figure 4. One can see that the distance between the centre of each tube arranged in a triangle pitch results in a triangle, where all edges are of the same length, providing that all angles are equal to 60°. The tubes staggered in a so-called 45° rotated square result in a square pattern where all angles are equal to 90°.

The distance between the centres of the staggered tubes is 25 mm, increasing the compactness. The central baffle spacing is 90 mm so that the baffles are mounted at locations with a circular cross-section on the double corrugated tubes. The main geometrical constraints of the reference heat exchanger and the heat exchanger analysed in this study are listed in Table 1. Note that the baffle cut, B_c, is the percentage of the shell cross-section area not covered by a baffle [26].

Table 1. Geometrical constraints.

Constraint	Present Study	Ref. [25]
Shell diameter, D, mm	100	90
Tube diameter, D_h, mm	20	20
Number of tubes, N_t	9	7
Heat exchanger length, l, mm	600	600
Number of baffles, N_b	6	6
Central baffle spacing, B_s, mm	90	86
Baffle cut, B_c, %	36	36
Bundle geometry, pitch length, PL, mm	45° rotated square, 25 mm	Triangle, 30 mm
Inlet/outlet diameter/length, l, mm	20/20	Not stated/not stated

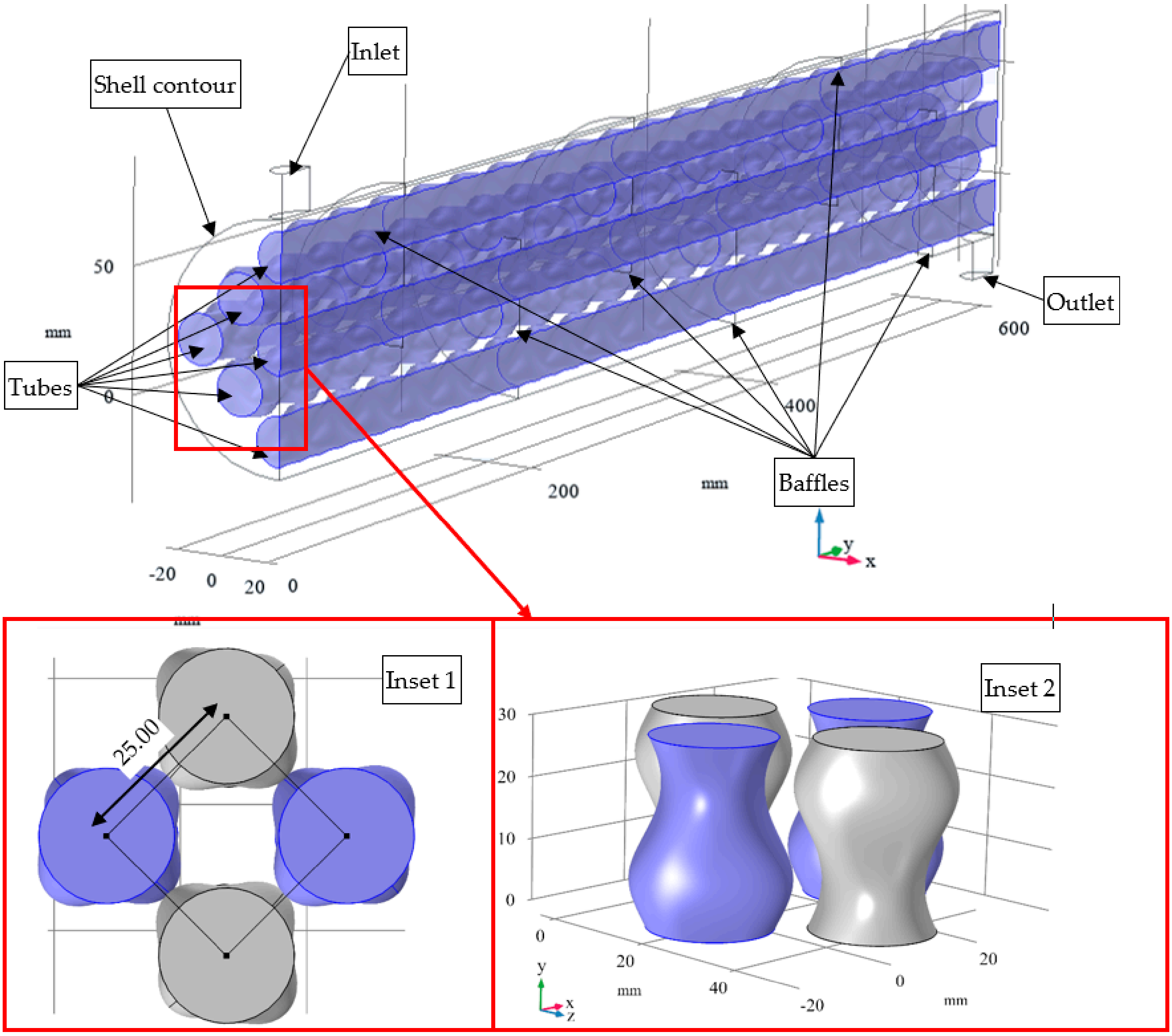

Figure 3. A heat exchanger with EAC AR16 K15D tubes with symmetry boundary conditions applied on the cut plane. (**Inset 1**) The tube bundle geometry is shown by the black dashed line. (**Inset 2**) A differential volume of the double corrugated tubes staggered into the bundle. The double corrugated tubes marked blue have been rotated 90° around their axes in order to increase the compactness of the tube bundle.

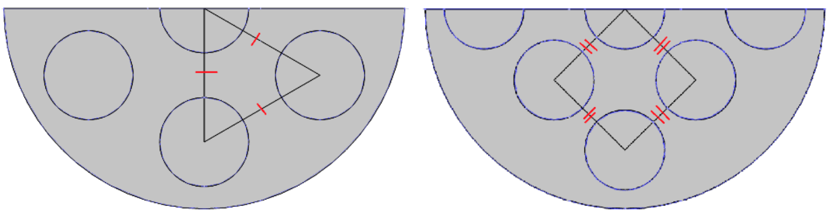

(**a**) (**b**)

Figure 4. Schematic of the tube arrangement inside the heat exchanger (HEX) analysed (**a**) in [25] and (**b**) this study.

The reconstructed heat exchanger described in [25] was solved using COMSOL Multiphysics steady state Conjugated Heat Transfer module, since the tube side was simulated as solid rods with constant surface temperature [25]. All modelling conditions applied in [25] and in the present study are summarised in Table 2. The heat transfer fluid was liquid water with temperature-dependent thermophysical properties available from the material library in COMSOL Multiphysics.

Table 2. Modelling conditions.

Parameter	Value
Mass flow rate, $\dot{m}$, kg/s	1
Tube wall temperature, T_w, K	450
Inlet water temperature, T_{in}, K	300
Specific heat capacity of the tube material, c_p, J/kg/K	49
Thermal conductivity of the tube material, k, W/m/K	14.3

Three types of turbulence models have been investigated in the present study. Namely, the standard k-ε, the realisable k-ε and the Shear Stress Transport (SST)turbulence models. As it was pointed out in [25], there is no rule which turbulence model should be used for HEX modelling, and different models could be more suitable than others in different studies. It is important to emphasise that the study presented in [25] was carried out using ANSYS Fluent, while the present study was carried out using COMSOL Multiphysics, which could also contribute to the difference in choosing the turbulence model. Thus, the HEX model reconstructed from [25] was simulated using all three turbulence models after adjusting the number of mesh elements for each model. On one hand, the realisable k-ε model was concluded to provide the best results for the study reported in [25]. On the other hand, the standard k-ε turbulence model was significantly less computationally expensive, i.e., it took approximately 5 h to solve the reconstructed full HEX model with 1.41 million mesh elements, while the realisable k-ε turbulence model took more than 28 h for the model with 1.36 million mesh elements. The SST turbulence model is a combination of the k-ε and the k-ω turbulence models providing better convergence than k-ω and better accuracy than k-ε [30]. However, the SST turbulence model took 96 h to converge. In addition, the results for net heat flux, q, obtained using all three turbulence models differ by only 6.7%. Moreover, the convergence of the reconstructed model was also improved when the standard k-ε turbulence model was used. It is also important to underline that the purpose of the present study was to compare the performance of the double corrugated tube geometry in a tube-in-shell HEX to that of the straight tubes. Therefore, due to the significant savings in computational power over fairly insignificant difference in obtained results, the standard k-ε turbulence model has been used to model HEXs analysed in this study. The results obtained on heat transfer in [25] and in this study are summarised in Table 3. Note that the convergence criteria in this study were 10^{-5} and 10^{-6} for the heat transfer residuals and for all the other residuals, respectively, and 10^{-6} and 10^{-3} for the pressure residuals and for all the other residuals, respectively, in [25].

One can see from Table 3 that the maximum difference in the simulation results obtained in [25] and in the present study are less than 10%. Thus, considering all the inevitable differences between the CFD models in [25] and this study, the obtained simulation results are considered to be in good agreement and the developed model is considered to be valid.

A mesh independence study was carried out for every modelled geometry. The grid convergence index, GCI, was calculated for each model as defined in Equations (3)–(8) [31–33]. Firstly, the order of convergence, p, of the model is determined as given in Equation (3).

$$p = \frac{\ln\left[\frac{q_3 - q_2}{q_2 - q_1}\right]}{\ln(r)} \quad (3)$$

where p is the order of convergence, q_1, q_2 and q_3 are the actual net heat flux obtained from simulations with the finest, second finest and third finest mesh, r is the mesh refinement ratio, calculated as in Equation (4).

$$r = \frac{ME_{i+1}}{ME_i} \tag{4}$$

where ME is the number of mesh elements.

Then the true value, q_t, at zero grid spacing is evaluated using the Richardson extrapolation as noted in Equation (5).

$$q_t = q_1 + \frac{q_1 - q_2}{r^p - 1} \tag{5}$$

Table 3. CFD results obtained for the reconstructed HEX.

Parameter	Ref. [25]	Present Study, Full Model	∣Difference w. r. t. Ref. [25]∣, %	Present Study, Model with Symmetry BC	∣Difference w. r. t. Ref. [25]∣, %
		Standard k-ε turbulence model			
Outlet temperature, T_o, K	330.00	335.13	1.55	335.32	1.61
Total heat transfer rate, q, kW	138.32	146.64	6.02	147.37	6.54
		Realisable k-ε turbulence model			
Outlet temperature, T_o, K	330.18	335.28	1.54	334.48	1.30
Total heat transfer rate, q, kW	131.79	148.07	12.35	143.78	9.10
		SST			
Outlet temperature, T_o, K	-	332.97	-	333.39	-
Total heat transfer rate, q, kW	-	138.78	-	141.08	-

Then GCI is calculated as given in Equation (6).

$$GCI_n = \frac{F_S \, |\varepsilon|}{r^p - 1} \tag{6}$$

where F_S is the safety factor and here it is 1.25, since p was evaluated using three meshes, ε is the relative error between two grids and is defined in Equation (7).

$$\varepsilon = \frac{q_i - q_{i+1}}{q_i} \tag{7}$$

Finally, it was checked if the solution is in the asymptotic range of convergence as defined in Equation (8).

$$GCI_{n+1} = r^p GCI_n \tag{8}$$

GCI can be considered as a relative error bound of how the obtained solution is far away from the asymptotic value and the safety factor, F_S, provides a 95% confidence interval [32]. The obtained results on GCI and asymptotic convergence, calculated according to Equation (8), are presented in Table 4 for each modelled HEX geometry.

Table 4. The results of the *GCI* (grid convergence index) analysis of each modelled geometry.

Name of HEX	$\mid GCI_{1\text{–}2} \mid$	$\mid GCI_{2\text{–}3} \mid$	Asymptotic Convergence (Equation (8))	True Value, q_t, kW	No. of Mesh el.
Straight	0.0204	0.0047	0.9874	157.95	771,383
EAC AR16 K15D	0.0632	0.0231	0.9695	182.75	1,358,884
EAC AR16 K30D	0.0547	0.0988	0.9631	152.74	796,612
EAC AR20 K15D	0.0583	0.0395	0.9854	200.98	2,089,290
EAC AR20 K30D	0.0118	0.0116	0.9906	367.69	2,320,316
EDH AR16 K15D	0.0467	0.0267	0.9846	202.96	2,660,826
EDH AR16 K30D	0.0037	0.0130	0.9925	169.43	1,518,398
EDH AR20 K15D	0.0739	0.1410	0.9430	177.38	1,194,197
EDH AR20 K30D	0.0473	0.0817	0.9714	143.57	1,955,813

Note that further mesh independence study seeking to obtain lower *GCI* values and asymptotic convergence closer to 1 would have led to unreasonably long computational time. The mass balance for all the analysed models was obtained within the error limit of 10^{-6}. Figure 5 shows a fragment of a mesh of an EDH AR20 K30D heat exchanger.

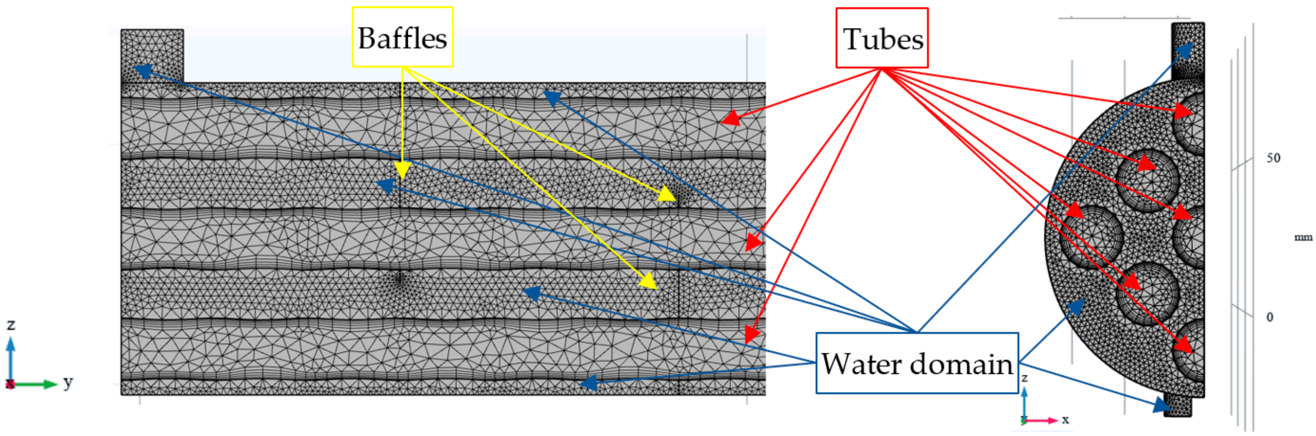

(**a**) (**b**)

Figure 5. Fragment of a mesh of an EDH AR20 K30D heat exchanger at (**a**) the symmetry plane and (**b**) the front plane of the heat exchanger.

The governing equations were formulated in Cartesian coordinates for an incompressible fluid with temperature-dependent thermophysical properties. Thus, the continuity equation may be written as in Equation (9).

$$\nabla \cdot \boldsymbol{u} = 0 \tag{9}$$

where $\boldsymbol{u}$ is the fluid velocity vector.

The momentum conservation equation is given by Equation (10).

$$-\rho(\boldsymbol{u} \cdot \nabla \boldsymbol{u}) = \nabla p - \mu \nabla^2 \boldsymbol{u} \tag{10}$$

where p is the pressure field, μ is the dynamic viscosity, ρ is the density.

The energy equation is given by Equation (11).

$$\rho\, c_p(\boldsymbol{u} \nabla T) = \nabla \cdot \boldsymbol{q} + \nabla \cdot (k \nabla T) + Q_{vd} \tag{11}$$

where q is the heat flux by conduction, Q_{vd} is the viscous dissipation defined by Equation (12) [34].

$$Q_{vd} = \tau : \nabla \boldsymbol{u} \tag{12}$$

where τ is the viscous stress tensor.

No-slip boundary conditions were applied on the solid walls, i.e., tube walls, shell walls and baffles. A solid wall is treated as a streamline with zero velocity by imposing no-slip boundary conditions, as can be seen in Equation (13).

$$\boldsymbol{u}\cdot\boldsymbol{n} = \boldsymbol{U}\cdot\boldsymbol{n} \tag{13}$$

where $\boldsymbol{U}$ is the velocity vector of the solid body and $\boldsymbol{n}$ is the unit normal to the surface of the solid body.

The main inputs of the model are the mass flow rate at a specified temperature and a specified wall temperature. The main model outputs are the resulting fluid temperature at the outlet and resulting pressure drop, Δp, through the heat exchanger. The performance of the analysed heat exchanger geometries was evaluated using the *NTU* method, which was selected over the log mean temperature difference method due to better suitability to represent heat exchanger design problems. The *NTU*, as expressed in Equation (14), is applicable for analysing heat exchangers where the ratio between heat capacity rates, C_R, is zero, or only one fluid is considered [35], as in this study.

$$NTU = -\ln(1-\varepsilon) \tag{14}$$

where ε is the effectiveness, which is defined by Equation (15) [36].

$$\varepsilon = \frac{q}{q_{max}} \tag{15}$$

where q is the actual net heat transfer rate obtained using the energy balance defined by Equation (16) [36], and q_{max} is the maximum available heat transfer rate, which would be obtainable if the heat exchanger would be infinitely long [35,36], defined by Equation (17).

$$q = \dot{m}_o c_p (T_o - T_i) \tag{16}$$

where T is the bulk fluid temperature at the inlet i and the outlet o of the heat exchanger and c_p is the specific heat capacity of the fluid.

$$q_{max} = C_{min}(T_{h,i} - T_{c,i}) \tag{17}$$

where C_{min} is the minimum heat capacity rate, which is defined by Equation (18). $T_{h,i}$ and $T_{c,i}$ are the hot and the cold fluid temperatures, respectively, at the inlets. Here $T_{h,i} = T_w$.

$$C_{min} = \dot{m}\, c_p \tag{18}$$

Equation (19) defines the pressure drop across the heat exchangers.

$$\Delta p = p_i - p_o \tag{19}$$

Thermal efficiency, η_t, of the analysed heat exchangers is compared using Equation (20).

$$\eta_t = \frac{q_c}{q_0} \tag{20}$$

where q is the actual net heat transfer obtained using Equation (16) and the subscripts c and 0 are corrugated and straight, respectively.

3. Results and Discussion

Data on the outlet temperature and the fluid flow velocity were obtained from the CFD simulations. The normalised pressure drop along the entire length of the selected HEX with straight and two sets of double corrugated tubes are shown in Figure 6. Note that Figure 6 shows the data only for the selected geometries in order to maintain the readability and clearness of the figure. The selected geometries demonstrated the lowest pressure drop and/or highest thermal effectiveness, which will be discussed further in this article. The full data set for each analysed geometry is available as supplementary data on http://dx.doi.org/10.17632/cdxvnh4ypr.1. The velocity and pressure drop data were acquired at a line in the middle of four neighbouring tubes of each heat exchanger as shown in Figure 6b and c. Note that the selected line crosses the analysed HEX in a way that it intersects with every baffle in the heat exchanger. One can see that, interestingly, the pressure drop as well as the fluid flow velocity for the HEX with straight tubes demonstrates the highest values, while the smallest pressure drop was obtained for the HEX with EDH AR16 K15D tubes. However, the maximum difference in the pressure drop between the two geometries is up to 10% and is obtained at the end of the HEX. Note that the periodic sharp jump in the pressure and periodicity of the fluid flow velocity is caused by the baffles placed every 90 mm along the HEX. From Figure 6 it is clear that the fluid flow is mostly affected by the baffles that contribute to the increase in pressure drop inside the heat exchanger, while the double corrugated geometry contributes to induced fluctuations of the fluid flow velocity.

In order to gain a better understanding of the flow behaviour inside the heat exchanger, the streamline plots shown in Figure 7 were analysed. Note that in Figure 7 are shown only the streamlines inside the heat exchangers analysed in Figure 6, while streamlines of the remaining geometries are presented in Figure A1 (Appendix A). One can see that the evaluation and comparison of the fluid flow velocity, thus pressure drop as well, are strongly dependent on the selected location in the heat exchanger. Figure 7 reveals that double corrugated tubes with shorter corrugation period, i.e., $k = 1.5{\cdot}D_\mathrm{h}$, create fluid flow regions with higher velocity, caused by the tube geometry. This induces the flow mixing which results in increased heat transfer. As it is seen from Figures 6 and 7, EDH AR20 K30D tubes induce regions and flow streams with higher velocity. However, this type of geometry somewhat hinders the creation of streamlines and re-circulation zones resulting in the smallest obtained pressure drop inside the heat exchanger. On the other hand, the HEX equipped with EDH AR20 K15D tubes induces regions with high fluid flow velocity as well as re-circulation zones, resulting in slightly higher pressure drop compared to the HEX with EDH AR20 K30D tubes. Nevertheless, the flow distortion in the HEX equipped with EDH AR20 K15D tubes results in the enhancement of the heat transfer.

Figure 8 shows the dependence of the thermal efficiency, η_t, on the fluid mass flow rate and the colour bar presents the *NTU* for each modelled case. Note that η_t presents the ratio between the thermal performance of the HEX with double corrugated tubes and the HEX with straight tubes as defined in Equation (20). Thus, $\eta_\mathrm{t} = 1$ is equivalent to the performance of the HEX equipped with straight tubes, which is emphasised as the dark horizontal line in Figure 8. Taking into consideration the velocity field data presented in Figure 7 and thermal efficiency data at $\dot{m} = 1.0$ kg/s in Figure 8, it is clear that the thermal efficiency of the heat exchangers equipped with double corrugated tubes that have a corrugation period $k = 1.5{\cdot}D_\mathrm{h}$ is up to 25% higher than the one with the straight tubes. This is due to the fluid flow mixing caused by the tube geometry. Heat exchangers equipped with double corrugated tubes that have a corrugation period $k = 3.0{\cdot}D_\mathrm{h}$ show increasing thermal efficiency with increasing mass flow rate. It is also noticeable that the thermal performance of the HEX equipped with double corrugated tubes EHD AR20 K30D increases slightly with increasing mass flow rate. It is worth mentioning that the thermal efficiency of the double corrugated tubes, experimentally evaluated in terms of Nusselt number for the internal flow, was up to six times higher than that of the straight tube [20]. It was demonstrated experimentally that the overall efficiency of the double corrugated tubes evaluated in terms of performance evaluation criterion, *PEC*, was up to 160% higher than that of the straight tube [20]. However, the thermal effectiveness of the double corrugated tubes, considering the external flow in HEX, is somewhat lower than for the internal flow. This could be attributed to the fact that the baffles cause significant fluid mixing, thus increasing the heat transfer on the outside of the tubes.

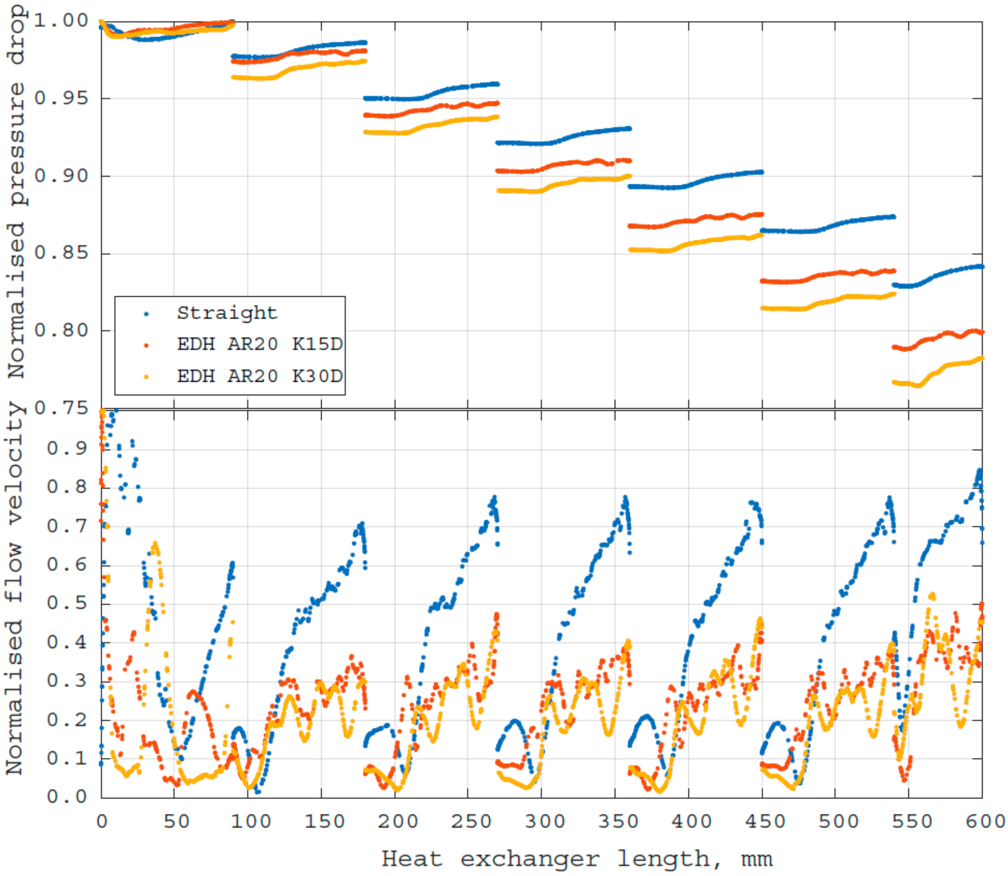

(**a**)

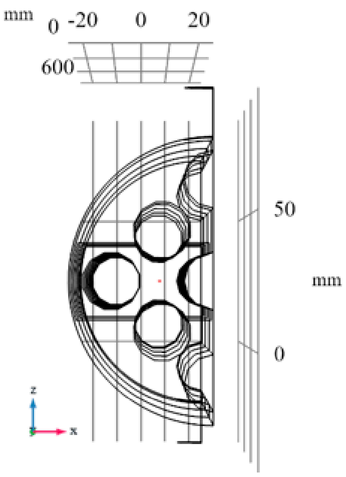

(**b**)

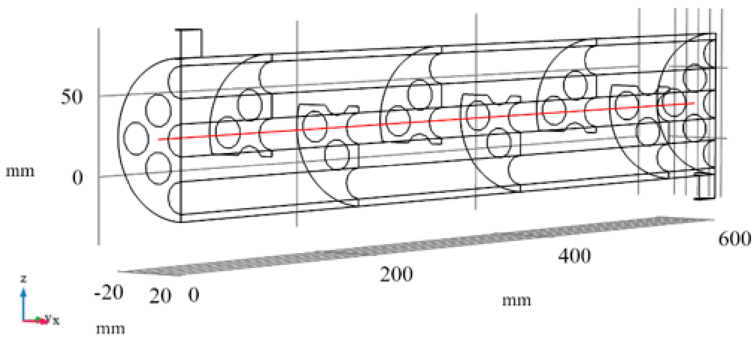

(**c**)

Figure 6. (**a**) Normalised pressure drop and normalised fluid flow velocity along the red solid line shown in (**b**) *z*-*x* plane and (**c**) axonometric view of the HEX.

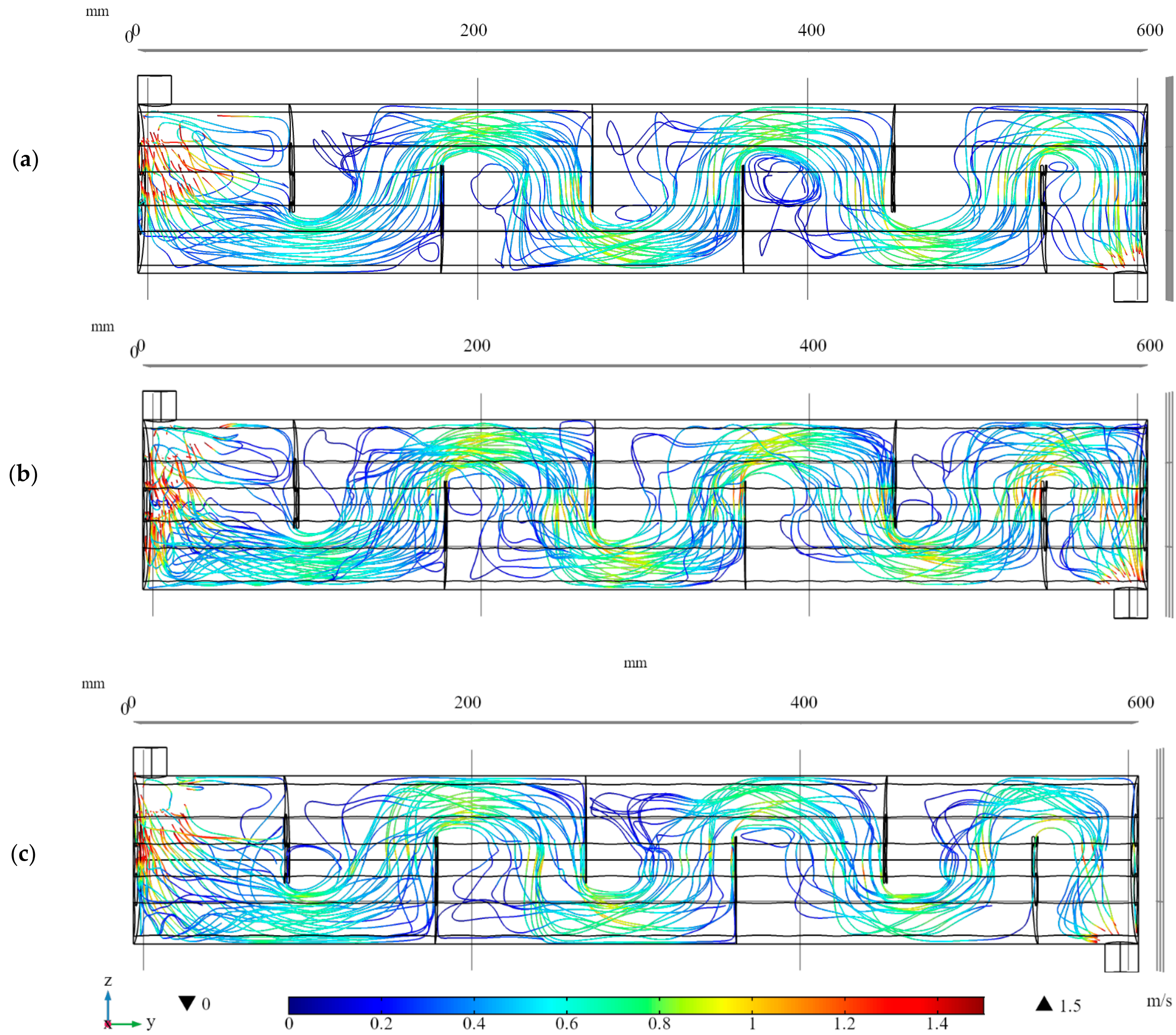

Figure 7. Streamlines at $\dot{m}$ = 1.0 kg/s for the heat exchanger fitted with (**a**) straight, (**b**) EDH AR20 K15P, (**c**) EDH AR20 K30P tubes.

Figure 9 presents the *ε-NTU* relation for all the analysed HEXs and the colour bar presents the mass flow rate for each modelled case. It is clear that the effectiveness, *ε*, and number of transfer units, *NTU*, is in almost all cases higher for heat exchangers equipped with double corrugated tubes. It should be emphasised that *NTU* decreases with increasing mass flow rate. This is because the fluid temperature at the outlet of the heat exchanger decreases with increasing mass flow rate, thus reducing the difference between the bulk fluid temperature at the inlet and outlet and therefore reducing the effectiveness of the heat exchangers.

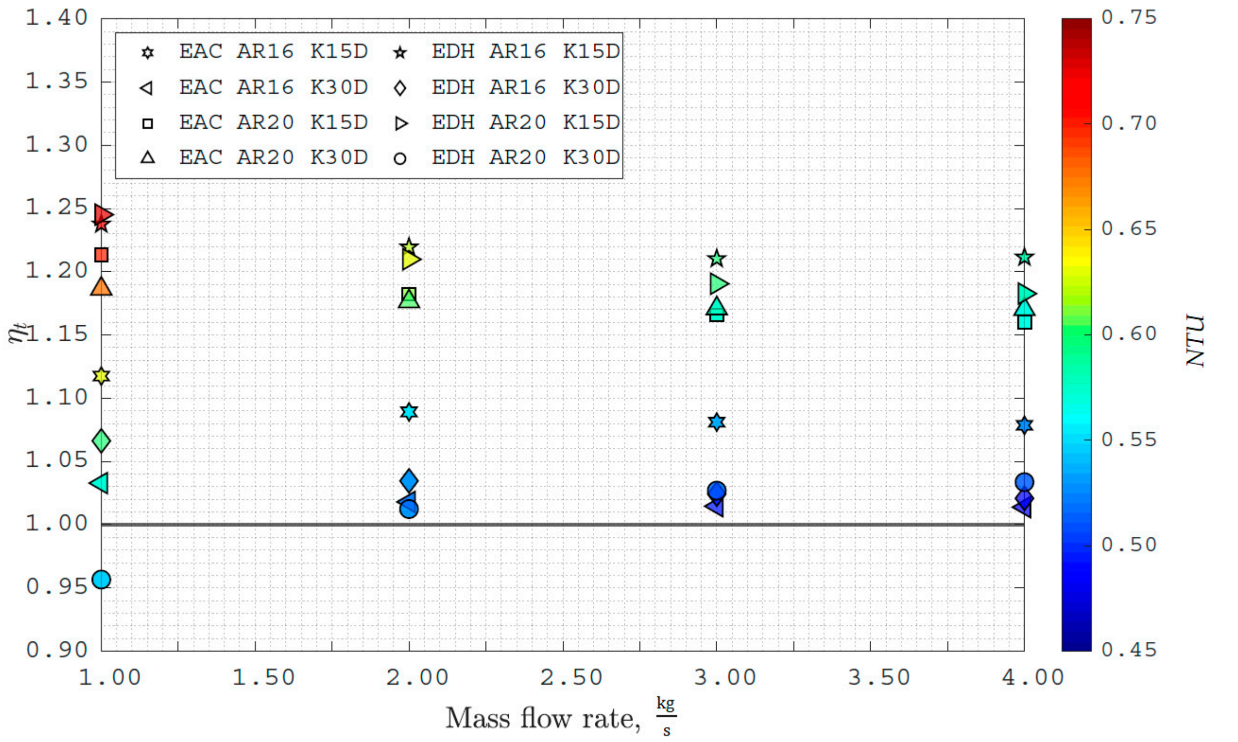

Figure 8. Thermal efficiency as a function of mass flow rate.

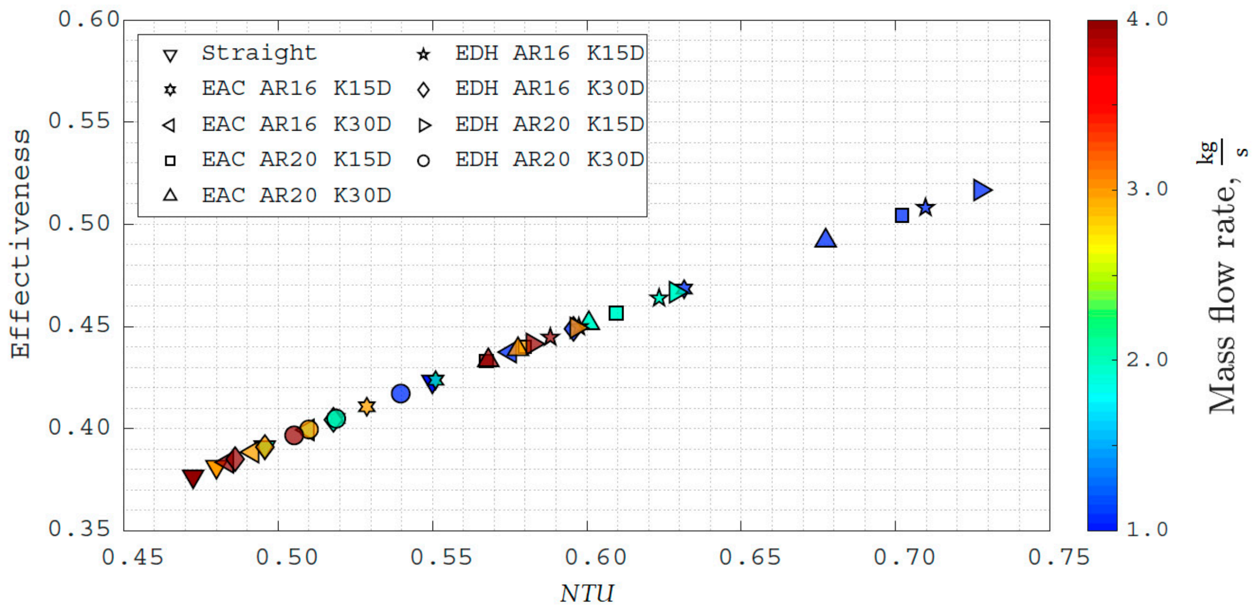

Figure 9. Effectiveness as a function of number of transfer units.

The full performance data of the analysed HEXs are summarised in Table 5.

Table 5. The CFD results of the analysed heat exchanger geometries.

Tube Name	Mass Flow Rate, $\dot{m}$, kg/s	Outlet Temperature, T_o, K	Net Heat Transfer, q, kW	NTU	Pressure Drop, Δp, kPa
Straight	1.0	338.17	160.57	0.55	22.94
	2.0	334.82	293.14	0.50	88.90
	3.0	333.80	426.91	0.48	197.16
	4.0	333.30	560.74	0.47	346.90
EAC AR16 K15D	1.0	343.01	179.43	0.63	20.69
	2.0	338.23	319.27	0.55	80.14
	3.0	336.84	461.52	0.53	177.70
	4.0	336.20	604.78	0.52	312.86
EAC AR16 K30D	1.0	339.56	165.85	0.58	18.99
	2.0	335.56	298.42	0.51	73.88
	3.0	334.40	433.15	0.49	164.05
	4.0	333.86	568.51	0.48	288.49
EAC AR20 K15D	1.0	346.76	194.83	0.70	19.74
	2.0	341.55	346.57	0.61	77.13
	3.0	339.77	497.70	0.58	171.66
	4.0	338.99	650.68	0.57	302.89
EAC AR20 K30D	1.0	345.50	190.52	0.68	17.63
	2.0	341.16	344.88	0.60	69.13
	3.0	339.76	499.87	0.58	153.93
	4.0	339.14	656.25	0.57	271.04
EDH AR16 K15D	1.0	347.72	198.72	0.71	20.40
	2.0	342.89	357.47	0.62	78.98
	3.0	341.32	516.67	0.60	175.37
	4.0	340.74	679.28	0.59	309.54
EDH AR16 K30D	1.0	340.70	171.22	0.60	19.83
	2.0	336.01	303.30	0.52	77.41
	3.0	334.60	437.24	0.50	172.14
	4.0	333.97	572.40	0.49	302.26
EDH AR20 K15D	1.0	348.07	199.93	0.73	20.47
	2.0	342.59	354.65	0.63	79.03
	3.0	340.67	508.22	0.60	175.41
	4.0	339.80	663.19	0.58	308.84
EDH AR20 K30D	1.0	336.33	153.61	0.54	17.17
	2.0	335.08	296.76	0.52	67.36
	3.0	334.55	438.40	0.51	150.24
	4.0	334.25	579.60	0.51	265.29

4. Conclusions

The CFD results obtained on a model of a small tube-in-shell heat exchanger equipped with straight and double corrugated tubes were presented. The simulations were compared in terms of thermal efficiency and *NTU*. The analysis demonstrates that suitably selected double corrugated tubes have the potential to enhance the performance of tube-in-shell heat exchangers by up to 25%. Moreover, the CFD results show that the main contribution to the pressure drop through the heat exchanger is created by the baffles, while the double corrugated geometry contributes more to the development of regions with increased fluid flow velocity between the baffles. This results in induced fluid mixing and enhanced heat transfer.

The simulation results demonstrate that a HEX equipped with EDH AR20 K30D tubes reduces pressure drop across the heat exchanger while still increasing the heat transfer compared to straight tubes. The advantage of using EDH AR20 K30D tubes in a tube-in-shell heat exchanger becomes more evident with increasing mass flow rate.

On the other hand, the highest increase in heat transfer was obtained with EDH AR16 K15D and EDH AR20 K15D geometries. The previous geometry demonstrates higher increase in heat transfer at mass flow rates $\dot{m} \geq 2$ kg/s, while the later one is more thermally efficient at lower mass flow rates. Interestingly, both geometries demonstrate rather similar pressure drop results that are slightly lower than for the straight tube geometry.

Taking into consideration previous work on the double corrugated tube geometry, it can be concluded that the double corrugated geometry has significantly higher impact on the fluid flow and heat transfer enhancement inside the double corrugated tubes, increasing their overall performance up to 160% [20]. Nevertheless, the increase in effectiveness of the double corrugated geometry in a tube-in-shell heat exchanger is seen from the CFD simulations performed in this study.

Author Contributions: Conceptualisation, K.N., M.P., K.E., C.R.H.B.; methodology, K.N.; software, K.N. and M.P.; validation K.N., M.P., K.E., C.R.H.B.; formal analysis, K.N.; investigation, K.N.; resources, M.P.; data curation, K.N.; writing—original draft preparation, K.N.; writing—review and editing, K.N., M.P., K.E., C.R.H.B.; visualisation, K.N.; supervision, K.E. and C.R.H.B. All authors have read and agreed to the published version of the manuscript.

Funding: This research received no external funding.

Data Availability Statement: The research data is available on doi:10.17632/cdxvnh4ypr.1.

Conflicts of Interest: The authors declare no conflict of interest.

Appendix A

(a)

(b)

(c)

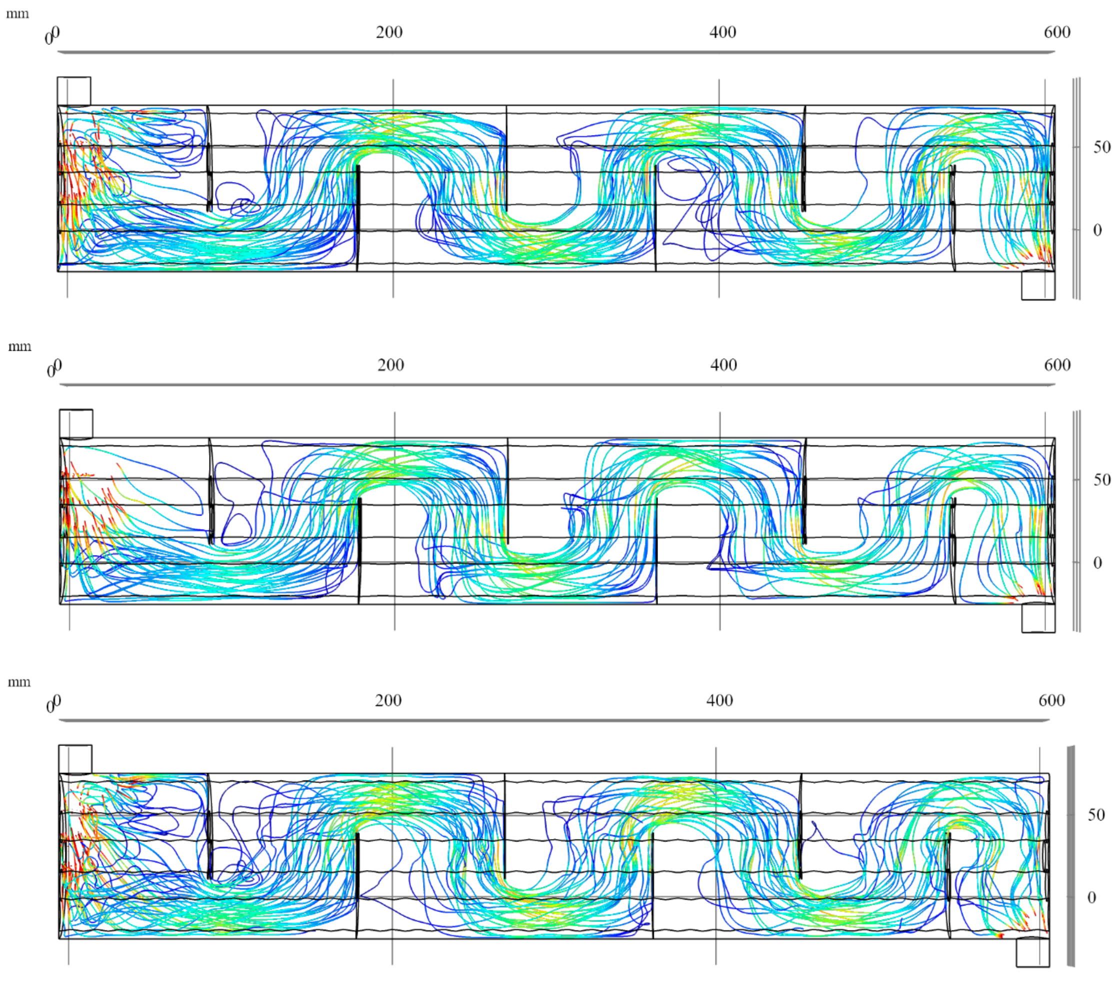

Figure A1. *Cont.*

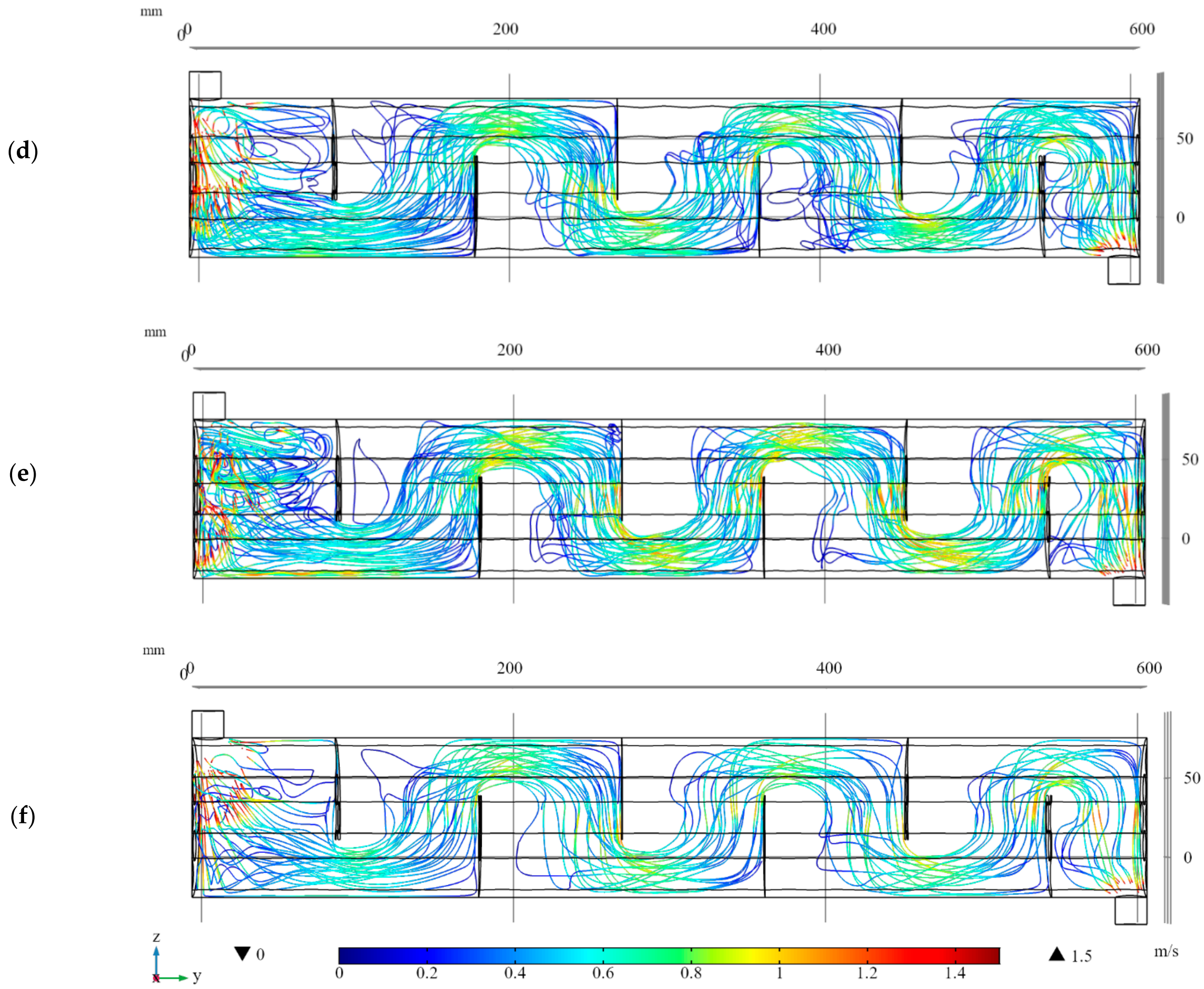

Figure A1. Streamlines at $\dot{m}$ = 1.0 kg/s for the heat exchanger fitted with (**a**) EAC AR16 K15D, (**b**) EAC R16 K30D, (**c**) EAC AR20 K15D, (**d**) EAC AR20 K30D, (**e**) EDH AR16 K15P, (**f**) EDH AR16 K30D tubes.

References

1. Rozzi, S.; Massini, R.; Paciello, G.; Pagliarini, G.; Rainieri, S.; Trifirò, A. Heat treatment of fluid foods in a shell and tube heat exchanger: Comparison between smooth and helically corrugated wall tubes. *J. Food Eng.* **2007**, *79*, 249–254. [CrossRef]
2. Carozza, A. Heat Exchangers in the Aviation Engineering. In *Heat Exchangers—Advanced Features and Applications*; InTech: London, UK, 2017; p. 38.
3. Sundén, B. Computational heat transfer in heat exchangers. *Heat Transf. Eng.* **2007**, *28*, 895–897. [CrossRef]
4. Kim, R.L.W.H. *Principles of Enhanced Heat Transfer*, 2nd ed.; Taylor and Francis group: Oxon, UK, 2006.
5. Laohalertdecha, S.; Naphon, P.; Wongwises, S. A review of electrohydrodynamic enhancement of heat transfer. *Renew. Sustain. Energy Rev.* **2007**, *11*, 858–876. [CrossRef]
6. Rainieri, S.; Bozzoli, F.; Pagliarini, G. Effect of a hydrophobic coating on the local heat transfer coefficient in forced convection under wet conditions. *Exp. Heat Transf.* **2009**, *22*, 163–177. [CrossRef]
7. Zachár, A. Analysis of coiled-tube heat exchangers to improve heat transfer rate with spirally corrugated wall. *Int. J. Heat Mass Transf.* **2010**, *53*, 3928–3939. [CrossRef]
8. Gee, D.L.; Webb, R.L. Forced convection heat transfer in helically rib-roughened tubes. *Int. J. Heat Mass Transf.* **1980**, *23*, 1127–1136. [CrossRef]
9. Bozzoli, F.; Cattani, L.; Mocerino, A.; Rainieri, S.; Tougri, I.; Colaço, M.J. Characterisation of the heat transfer in displaced enhancement devices by means of inverse problem approach applied to IR images. *Quant. Infrared Thermogr. J.* **2019**, 1–19. [CrossRef]
10. Eiamsa-ard, S.; Thianpong, C.; Eiamsa-ard, P.; Promvonge, P. Thermal characteristics in a heat exchanger tube fitted with dual twisted tape elements in tandem. *Int. Commun. Heat Mass Transf.* **2010**, *37*, 39–46. [CrossRef]
11. Bhuiya, M.M.K.; Chowdhury, M.S.U.; Shahabuddin, M.; Saha, M.; Memon, L.A. Thermal characteristics in a heat exchanger tube fitted with triple twisted tape inserts. *Int. Commun. Heat Mass Transf.* **2013**, *48*, 124–132. [CrossRef]

12. Dagdevir, T.; Ozceyhan, V. An experimental study on heat transfer enhancement and flow characteristics of a tube with plain, perforated and dimpled twisted tape inserts. *Int. J. Therm. Sci.* **2021**, *159*. [CrossRef]
13. Kareem, Z.S.; Jaafar, M.N.M.; Lazim, T.M.; Abdullah, S.; Abdulwahind, A.F. Heat transfer enhancement comparison in different tube shapes. *Int. Rev. Model. Simulations* **2015**, *8*, 232–240. [CrossRef]
14. Kareem, Z.S.; Jaafar, M.N.M.; Lazim, T.M.; Abdullah, S.; Abdulwahid, A.F. Heat transfer enhancement in two-start spirally corrugated tube. *Alexandria Eng. J.* **2015**, *54*, 415–422. [CrossRef]
15. Bozzoli, F.; Cattani, L.; Rainieri, S. Cross-helix corrugation: The optimal geometry for effective food thermal processing. *Int. J. Heat Mass Transf.* **2020**, *147*, 118874. [CrossRef]
16. Penzel, M.; Zinecker, M.; Schubert, A.; Hackert-Oschätzchen, M.; Ludwig, A.; Adamczewski, A.; Schulz, A.; Lausberg, M. Investigation of Forced Convection in Pin Structured Cold Plates for Improved Heat Transfer and Heat Spreading. In Proceedings of the 9th World Conference on Experimental Heat Transfer, Fluid Mechanics and Thermodynamics, Iguazu Falls, Brazil, 11–15 June 2017.
17. Kareem, Z.S.; Abdullah, S.; Lazim, T.M.; Jaafar, M.N.M.; Wahid, A.F.A. Heat transfer enhancement in three-start spirally corrugated tube: Experimental and numerical study. *Chem. Eng. Sci.* **2015**, *134*, 746–757. [CrossRef]
18. Khaboshan, H.N.; Nazif, H.R. Investigation of heat transfer and pressure drop of turbulent flow in tubes with successive alternating wall deformation under constant wall temperature boundary conditions. *J. Brazil. Soc. Mech. Sci. Eng.* **2018**, *40*, 1–16. [CrossRef]
19. Guo, Z.Y.; Li, D.Y.; Wang, B.X. A novel concept for convective heat transfer enhancement. *Int. J. Heat Mass Transf.* **1998**, *41*, 2221–2225. [CrossRef]
20. Navickaitė, K.; Mocerino, A.; Cattani, L.; Bozzoli, F.; Bahl, C.; Liltrop, K.; Zhang, X.; Engelbrecht, K. Enhanced heat transfer in tubes based on vascular heat exchangers in fish: Experimental investigation. *Int. J. Heat Mass Transf.* **2019**, *137*, 192–203. [CrossRef]
21. Navickaitė, K.; Cattani, L.; Bahl, C.R.H.; Engelbrecht, K. Elliptical double corrugated tubes for enhanced heat transfer. *Int. J. Heat Mass Transf.* **2019**, *128*, 363–377. [CrossRef]
22. Prithiviraj, M.; Andrews, M.J. Three dimensional numerical simulation of shell-and-tube heat exchangers. Part I: Foundation and fluid mechanics. *Numer. Heat Transf. Part A Appl.* **1998**, *33*, 799–816. [CrossRef]
23. Prithiviraj, M.; Andrews, M.J. Three dimensional numerical simulation of shell-and-tube heat exchangers. Part II: Heat transfer. *Numer. Heat Transf. Part A Appl.* **1998**, *33*, 817–828. [CrossRef]
24. Kumar, V.; Saini, S.; Sharma, M.; Nigam, K.D.P. Pressure drop and heat transfer study in tube-in-tube helical heat exchanger. *Chem. Eng. Sci.* **2006**, *61*, 4403–4416. [CrossRef]
25. Ozden, E.; Tari, I. Shell side CFD analysis of a small shell-and-tube heat exchanger. *Energy Convers. Manag.* **2010**, *51*, 1004–1014. [CrossRef]
26. Shah, R.K.; Sekulic, D.P. *Fundamentals of Heat Excanger Design*; John Wiley & Sons: Hoboken, NJ, USA, 2003.
27. Wegner, N.C.; Snodgrass, O.E.; Dewar, H.; Hyde, J.R. Whole-body endothermy in a mesopelagic fish, the opah, Lampris guttatus. *Science* **2015**, *348*, 786–789. [CrossRef]
28. Dickson, K.A.; Graham, J.B. Evolution and consequences of endothermy in fishes. *Physiol. Biochem. Zool.* **2004**, *77*, 998–1018. [CrossRef] [PubMed]
29. Navickaitė, K.; Mocerino, A.; Cattani, L.; Bozzoli, F.; Bahl, C.R.H.; Engelbrecht, K. Heat transfer in double corrugated tubes. In Proceedings of the 9th International Conference & Workshop REMOO-2019, Hong Kong, China, 16–18 April 2019.
30. Frei, W. Which Turbulence Model Should I Choose for My CFD Application? 2017. Available online: https://www.comsol.de/blogs/which-turbulence-model-should-choose-cfd-application/ (accessed on 28 December 2020).
31. Slater, J.W. Examining Spatial (Grid) Convergence. 2008. Available online: https://www.grc.nasa.gov/WWW/wind/valid/tutorial/spatconv.html (accessed on 1 February 2021).
32. Kwasniewski, L. Application of grid convergence index in FE computation. *Bull. Pol. Acad. Sci. Tech. Sci.* **2013**, *61*, 123–128. [CrossRef]
33. Hærvig, J.; Sørensen, K.; Condra, T.J. On the fully-developed heat transfer enhancing flow field in sinusoidally, spirally corrugated tubes using computational fluid dynamics. *Int. J. Heat Mass Transf.* **2017**, *106*, 1051–1062. [CrossRef]
34. ComsolMultiphysics. *Heat Transfer Module User's Guide*; Comsol: Burlington, MA, USA, 2015; pp. 1–222.
35. Nellis, G.; Klein, S. *Heat Transfer*, 2nd ed.; Cambridge University Press: New York, NY, USA, 2009.
36. Bergman, T.L.; Lavine, A.S.; Incropera, F.P.; Dewitt, D.P. *Introduction to Heat Transfer*, 6th ed.; John Wiley & Sons: Jefferson City, MO, USA, 2011.